Capillarity

Vol. 11, No. 3, p. 70-80, 2024

Original article

Effects of salinity and driving pressure on water imbibition during shale formation

Xianyu Shao[1], Ke Wang[1]*, Lingyun Zhao[1,2], Chao Su[3], Daquan Zhang[2], Wei Gao[4]

[1]*College of Resources and Environmental Engineering, Key Laboratory of Karst Georesources and Environment, Ministry of Education, Guizhou University, Guiyang 550025, P. R. China*

[2]*Guizhou Engineering Research Institute of Oil & Gas Exploration and Development, Guiyang 550001, P. R. China*

[3]*Geological Exploration and Development Research Institute, CNPC Chuanqing Drilling Engineering Co., Ltd., Chengdu 610051, P. R. China*

[4]*Guizhou Engineering Technology Research Center for Coalbed Methane and Shale Gas, Guiyang 550009, P. R. China*

Keywords:
Imbibition
handy model
osmotic pressure
driving pressure
initial water saturation

Cited as:
Shao, X., Wang, K., Zhao, L., Su, C., Zhang, D., Gao, W. Effects of salinity and driving pressure on water imbibition during shale formation. Capillarity, 2024, 11(3): 70-80.
https://doi.org/10.46690/capi.2024.06.02

Abstract:
During the construction stage of underground engineering projects, the engineering fluids used often carry a certain level of pressure, and rock formations in the subsurface invariably contain fluids with a certain degree of salinity. Both the driving pressure in engineering fluids and the high degree of salinity in the original subsurface fluids will inevitably impact the entire imbibition process; however, despite the high relevance to actual engineering situations, these effects have not been systematically studied in traditional researches on imbibition. In this study, imbibition experiments under varying engineering conditions, such as water salinity, driving pressure and initial water saturation, are conducted to detect the actual imbibition phenomenon in underground engineering projects. In addition, a modified Handy model considering the above three factors is proposed to better predict the imbibition law of shale under actual engineering conditions. The results show that salinity and driving pressure have significant effects on water imbibition, while the modified model, possessing exceptionally high fitting accuracy, effectively characterizes the forced imbibition patterns of shale. This study provides new insights into investigating fluid imbibition phenomena in the development stage of underground engineering.

1. Introduction

Many types of engineering applications involve artificially injecting fluids into the formation, such as fracturing, drilling, water injection (Li et al., 2022), the circulation and reflux of geothermal fluids (Wang et al., 2012), underground carbon dioxide, and other energy storage (Gao et al., 2018). In the practical underground industry, a large amount of liquid is often injected into tight formations and imbibed into tight rock pores under pressure and other spontaneous imbibition forces, a process called forced imbibition, which is different from spontaneous imbibition and displacement. Spontaneous imbibition is a natural phenomenon that occurs in micro- and nano-scale pores and is mainly driven by capillary force (Abd et al., 2019; Yuan et al., 2019; Hu et al., 2020; Deng and Pan, 2021). Displacement primarily occurs in macroscopic pores and is mainly the result of pressure difference. Both spontaneous and forced imbibition take place within micro- and nano-scale porous media, with capillarity being the primary driving force, and osmotic pressure likely being a secondary driving pressure. In engineering applications regarding underground tight rock formations, the spontaneous imbibition theory fails to accurately describe liquid flow and imbibition processes. However, when the driving pressure and the osmotic pressure are considered, the process and patterns of foreign fluid entering the underground rock pores under engineering

Yandy Scientific Press

*Corresponding author.
E-mail address: s15520592163@126.com (X. Shao); kwang5@gzu.edu.cn (K. Wang); zhaolingyun-554@163.com (L. Zhao); shuc_dyy@cnpc.com.cn (C. Su); daquan0807@163.com (D. Zhang) gaoweicumt@126.com (W. Gao).

Received February 28, 2024; revised March 20, 2024; accepted April 13, 2024; available online April 18, 2024.

conditions can be accurately described.

Imbibition is influenced by various factors such as interfacial tension, wettability, fluid viscosity, pore size and roughness, initial water saturation, etc. However, the effects of driving pressure and the salinity difference between formation water and fracturing fluid are also important due to the high-pressure fracturing in shale reservoirs. In the past decade, the imbibition characteristics of shales have been analyzed by considering different influencing factors. Schmid and Geiger (2012) argued that chemical-osmosis, thermal osmosis, and capillarity are all non-negligible driving forces in the process of imbibition. Ghanbari and Dehghanpour (2015) found that initial water saturation decreases water uptake. Zhou et al. (2016) investigated the effects of both capillary and osmotic diffusion as the key mechanisms in fluid imbibition through simultaneous imbibition experiments, and the results illustrated that the contact angle and salinity of shale rock can influence the imbibed rate and the imbibition process is dominated by both capillary and osmotic diffusion. Xu et al. (2018) carried out comparative imbibition experiments and revealed that the ultimate oil/gas recovery by forced imbibition is significantly improved when compared to that by spontaneous imbibition.

The traditional Lucas-Washburn (L-W) model and its modified versions are widely used to describe the imbibition characteristics (Cai et al., 2014). The traditional L-W model is based on the imbibition of the wetting phase in a cylindrical tube with a smooth surface. This model is only applicable to vertical capillary tubes with uniformly circular interiors (Lucas, 1918; Washburn, 1921). Benavente et al. (2002) improved the traditional L-W model by introducing factors related to the rock microstructure. However, there are still limitations because the improved model assumes that all pores in a porous medium are the same. Zeng et al. (2020) modified the Hagen-Poiseuille equation and incorporated the slip length, viscosity, wettability, and nano-size; however, the revised model was still insufficient for engineering applications due to overlooking the forced process. Some scholars have considered more complex micro-scale imbibition phenomena. Wang et al. (2022b) established a dynamic imbibition model of penny-shaped blind pores while considering the factor of desorption resistance of adsorbed and free gases. Neunkirchen et al. (2022) modified the L-W model by incorporating the porous tube model and accounting for gravity, resulting in an easy-to-handle method for characterizing capillary rise. A et al. (2022) modified the classical L-W model by incorporating the Cox-Voinov law to account for the effects of dynamic contact angles. This model accurately represents the imbibition dynamics involved in the growth of imbibition length, dynamic contact angle, and interface velocity. Due to taking account the details of pore structure and gas-water flow patterns, the L-W model performs better when applied to single-pore or capillary bundle models. However, in the field of underground engineering where rock pore structures are complex and homogeneous, the application of the L-W model is not convenient because it requires many parameters.

The Handy model is another widely used imbibition model (Handy, 1960). Compared to the L-W model, it overlooks the details such as pore structure and gas-water interface properties, increasing its convenience for engineering applications. The Handy model is derived based on the assumption of a piston-shaped imbibition profile where the mass/volume of imbibed water is proportional to the square root of the imbibition time. In recent years, many scholars have made improvements and modifications to the traditional Handy model (Table 1). Cai et al. (2014) developed improved Hagen-Poiseuille and Laplace-Young equations to derive a generalized model of spontaneous imbibition in porous media. This model takes into account all properties of the porous media and the wetting solution, as well as their interactions, which control the spontaneous imbibition process. Nonetheless, this model is not applicable to the forced imbibition process. Zhao et al. (2021) developed a porous fractal model for shale imbibition that considers capillary force, osmotic pressure and pore structure. Their study concluded that clay pores exhibit a greater increase in imbibition capacity under osmotic pressure compared to imbibition capacity under capillary force. Wang et al. (2022a) studied the effects of boundary conditions and initial water saturation on imbibition in saturated oil sands, improving the understanding of the effects of the two factors on spontaneous imbibition. Li et al. (2022) compared the dynamics of spontaneous imbibition and forced imbibition in a single capillary tube, and proposed semi-analytical solution models considering forced pressure and osmotic pressure. An important drawback of the traditional Handy model is its unsuitability for forced imbibition processes of shale, as it does not consider driving pressure and osmotic pressure.

Recently, domestic and foreign scholars have conducted extensive research on the mechanism of imbibition using various experimental methods. The balance-weighting method has proven to be a simple and widely used technique for measuring the core mass. It involves using balances and other instruments to calculate the amount of fluid drawn into the core and allows continuous measurements to obtain data curves. This method has been commonly used in imbibition experiments conducted in unconventional reservoirs. Among these methods, the traditional balance-weighting experiment is among the frequently used approaches to study the imbibition phenomenon in porous media (Ghanbari and Dehghanpour, 2015; Gao et al., 2019). Certain new techniques have also been implemented in experimental studies of imbibition. Lai et al. (2016) combined the imbibition experiment with Nuclear Magnetic Resonance testing to analyze the law of fluid flow in shale core samples at the pore level. Gruener et al. (2016) utilized neutron imaging technology not only to reveal the filling dynamics that follow the square root time dependence but also to indicate that the overall width of the imbibition front follows the time dependence. Hassan et al. (2017) demonstrated through shale imbibition experiments that radio frequency identification devices can be used for the non-contact measurement of fluid composition. Chakraborty et al. (2017) provided quantitative experimental evidence of water migration through common shale core plugs using micro-CT imaging, as well as evidence of clay expansion further impeding gas flow. Despite numerous theoretical studies of the imbibition phenomenon, few experiments have been conducted

Table 1. Several improved Handy percolation models.

References	Equation	Advantages	Limitations
Cai et al. (2014)	$Q^2 = \xi \frac{\rho^2 A^2 \phi^2 r (S_{wf} - S_{wi})^2 \sigma \cos\theta}{2\mu_w} t$	The initial wetting phase saturation is considered.	Unsuitable for forced imbibition.
Zhao et al. (2021)	$Q = A\phi \sqrt{\frac{2\sigma\cos\theta(w+6L_s) + \varepsilon E_0 RT(C_t - C_f)(w^2 + 6L_s w)}{6\mu_w} t}$	The effect of osmotic pressure on imbibition is considered.	Unsuitable for forced imbibition.
Wang et al. (2022b)	$Q = A \sqrt{\frac{2\phi K (S_{wf} - S_{wi}) P_c}{\frac{\mu_o}{k_{ro}} + \frac{\mu_w}{k_{rw}}} t}$	Oil viscosity and initial water saturation are considered.	Unsuitable for forced imbibition.
Li et al. (2022)	$Q = A\phi \frac{2\mu_0 L - \sqrt{4(\mu_0 L)^2 + (\mu_w - \mu_0)\left[r^2(P_f + P_\pi) + 2\sigma r\cos\theta\right] t}}{2(\mu_0 - \mu_w)}$	Forced pressure and osmotic pressure are considered.	The effect of initial water saturation is not considered.

Notes: Q denotes the imbibition volume, ξ denotes the composite parameter, ρ denotes the wetting liquid density, A denotes the cross-sectional area, ϕ denotes the porosity, r denotes the pore radius, S_{wf} denotes the water saturation after imbibition, S_{wi} denotes the initial water saturation, σ denotes the the surface tension, θ denotes the contact angle, μ_w denotes the viscosity of the water phase, t denotes the imbibition time, w denotes the clay pore width, L_s denotes the boundary slip length, ε denotes the number of ions after solute ionization, E_0 denotes the membrane efficiency, T denotes the absolute temperature of formation, R denotes the gas constant, C_t denotes the molar solute concentration in the original formation water, C_f denotes the molar solute concentration in the fracturing fluid, K denotes the permeability, P_c denotes the capillary pressure, k_{ro} denotes the Relative permeability of oil, k_{rw} denotes the relative permeability of water, μ_0 denotes viscosity of the oil phase, L denotes length of a single-layer capillary tube, P_π denotes the osmotic pressure, P_f denotes the driving pressure.

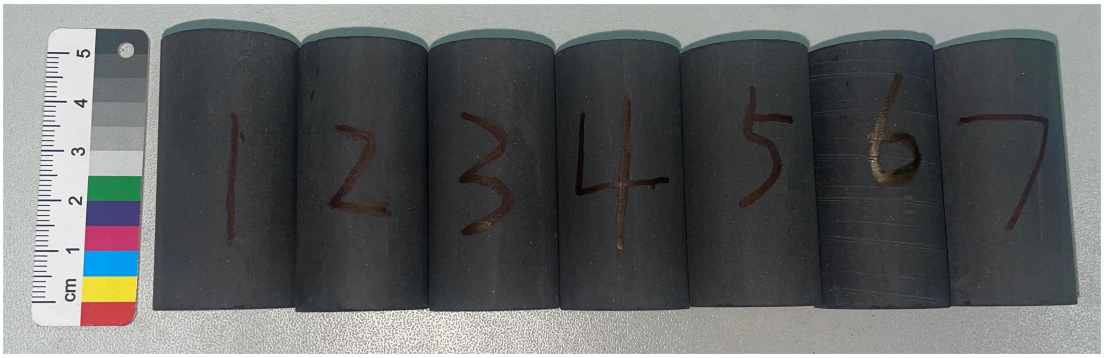

Fig. 1. Seven shale core samples for the imbibition experiment.

on the process of forced imbibition of shale.

This study aimed to explore the factors influencing imbibition capacity and make up for the deficiencies of existing imbibition models. Firstly, three key factors, osmotic pressure, driving pressure, and initial water saturation, were analyzed through multiple groups of imbibition experiments, and then an improved Handy model was proposed by introducing these key parameters. Finally, the feasibility of the improved model was verified through imbibition experiments on seven sets of shale core samples and compared with existing imbibition models. The results show that the new model has high fitting accuracy.

2. Experiments

2.1 Materials and device design

2.1.1 Sample preparation and petrological measurements

The shale samples were obtained from Qianbei district, Guizhou Province, China. Seven parallel core samples, labeled S1-S7 (Fig. 1), were drilled perpendicularly to the stratigraphic direction. Each core sample had a diameter of 2.5 cm and a height of approximately 5 cm. The residual fragments were used for basic physical and petrological analyses, including nitrogen porosity, pulse attenuation permeability, etc.

2.1.2 Contact angle experiment

The contact angles of core samples were obtained using deionized water and a high-resolution camera. For this measurement, a water droplet was placed on the polished and clean surface of the shale core. A graduated syringe was used to ensure that the volume of water droplets is the same. Finally, contact angles were measured in four different directions for

Table 2. Petrophysical properties of the shale sample.

Sample	Diameter (mm)	Height (mm)	Contact angle (°)	Drying quality (g)
S1	25.02	50.93	50.53	63.5934
S2	24.92	50.48	49.56	63.4141
S3	25.01	50.57	48.97	63.4283
S4	25.04	50.68	51.25	63.4581
S5	24.95	50.41	55.41	63.3965
S6	25.06	50.65	53.32	63.4780
S7	25.02	50.63	49.58	63.5312

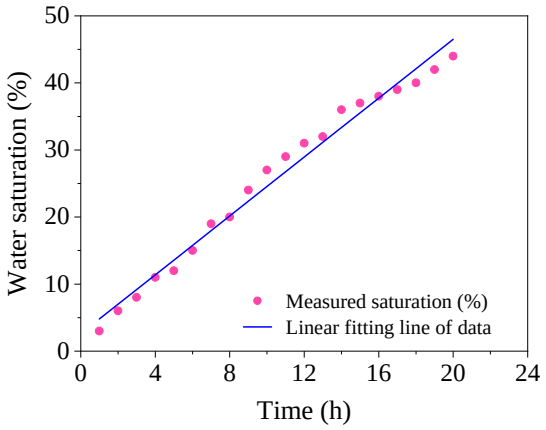

Fig. 2. Relationship curve of equilibrium time and water saturation.

a single sample to obtain the average value.

The physical parameters of the shale samples are shown in Table 2. Since all seven core samples were taken from the same shale slab, only one set of data is shown. The porosity (3.41%) and permeability (2.30×10^{-6} D) properties of the shale indicate that it is a typical dense reservoir rock. The average contact angle of the sample is 51.23°, and the average drying quality is 63.4714 g.

2.2 Imbibition experiment

In order to study the effects of osmotic pressure, driving pressure and initial water saturation on shale imbibition action, two experimental devices were designed to conduct imbibition experiments on seven samples under different conditions (Table 3). The entire experimental process was performed at normal temperature and pressure, with distilled water as the experimental fluid.

2.2.1 Imbibition experiment considering initial water saturation

Imbibition experiments by S2 and S3 samples were conducted with different water saturation levels, and the adsorption equilibrium method was firstly used to establish the original water saturation under stratigraphic conditions. During the experiment, shale samples were placed in a water vapor environment. The experimental steps were as follows:

Table 3. Experimental design parameters.

Sample	Osmotic pressure (MPa)	Driving pressure (MPa)	Initial water saturation (%)
S1	0	0	0
S2	0	0	10
S3	0	0	20
S4	0	0.1	0
S5	0	0.2	0
S6	0.33	0	0
S7	0.66	0	0

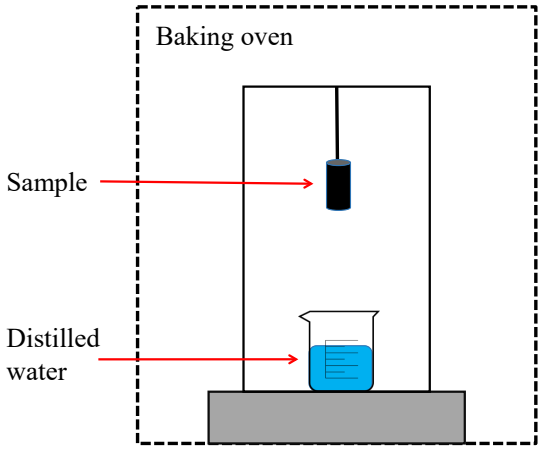

Fig. 3. Layout of device for establishing water saturation in rock cores.

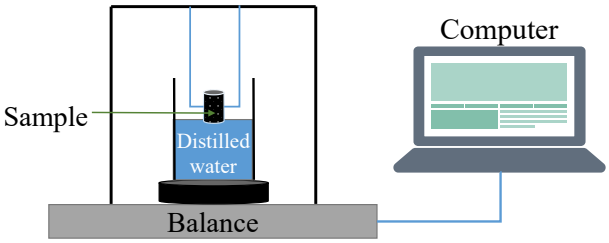

Fig. 4. Imbibition experiment using device-I.

1) The sample is placed into a container containing distilled water (Fig. 2);
2) The container is heated to 105 °C to form a water vapor environment, then the sample is removed and weighed at the set time;
3) Steps 1) and 2) are repeated, and the curves of different equilibratioon times versus the initial water saturation of samples are established (Fig. 3).

The equilibrium time was controlled to achieve different water saturation states of the sample. Finally, imbibition experiments with different initial water saturation levels were conducted by the two sets of samples using device-I under normal temperature and pressure conditions (Fig. 4).

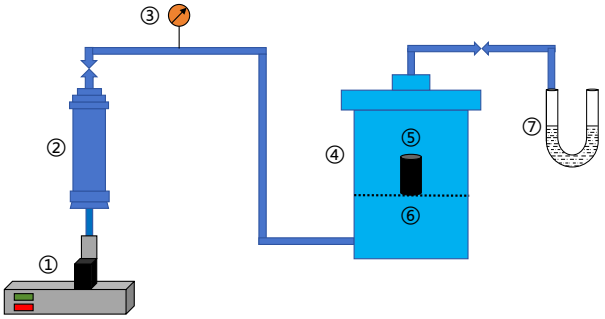

Fig. 5. Imbibition experimental device-II: ① High-pressure pump; ② water pump; ③ pressure gage; ④ imbibition container; ⑤ core; ⑥ wire mesh bracket and ⑦ u-tube.

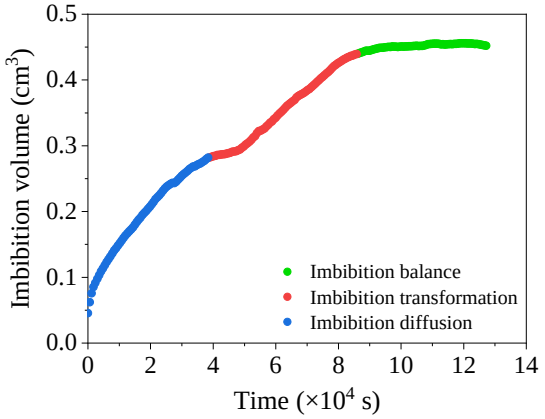

Fig. 6. Imbibition experimental curve of the dry sample.

2.2.2 Imbibition experiment considering osmotic pressure

These experiments were carried out with samples S4 and S5 under vacuum conditions, and the samples were subsequently placed in an oven and dried at 60 ± 5 °C for 24 hours (avoiding damage to clay minerals), so that the shale samples had the corresponding salt solution concentration. Using device-I, two sets of samples were subjected to imbibition experiments under normal temperature and pressure conditions. The samples were placed in a beaker filled with distilled water, and the water in the beaker was absorbed by the samples. The reduced mass on the balance was the imbibition volume of the samples. The imbibition volume for a certain period could be read out by a connected computer. Thus, the relationship between shale imbibition volume and time under different osmotic pressure conditions could be obtained.

2.2.3 Imbibition experiment considering driving pressure

In order to investigate the effect of driving pressure on shale imbibition action, an imbibition experimental device-II (Fig. 5) was designed independently to carry out forced imbibition experiments with samples S6 and S7. Firstly, the core samples were placed on the wire mesh bracket of the imbibition container, the container was pressurized to the set pressure and then the imbibition process was initiated. At this time, the whole imbibition container and the measuring cylinder were filled with deionized water, the reading of the U-tube every ten minutes was recorded, and reading was stopped once the value stabilized. The relationship between shale imbibition volume and time was obtained under different driving pressure conditions.

3. Results

The shale imbibition experiment, described in Section 2.2, was executed to obtain the imbibition curve (Fig. 6) based on the changes in rock sample quality at different times, which clarified the characteristics of shale imbibition. The results showed that the imbibition rate of the seven samples gradually decreased with time. After 33 h, the imbibition rate was close to zero, indicating that the sample had reached saturated state. The final imbibition volumes of the seven samples are given in Table 4.

According to the variation law of imbibition volume over time, the imbibition curve can be divided into three stages, as shown in Fig. 6: Imbibition diffusion stage, imbibition transformation stage, and imbibition balance stage. Among them, the imbibition diffusion stage is the main period that affects the imbibition ability. Fig. 7 depicts the relationship curve between imbibition volume and time for six shale samples under different experimental conditions. The curves show significant differences in the imbibition capabilities of the samples in line with variations in the experimental conditions.

Table 4. Final imbibition volumes of the samples under different experimental conditions.

Sample	Experimental condition	Final imbibition volume (cm^3)
S1	Normal temperature and pressure	0.4073
S2	$S_{wi} = 10\%$	0.3855
S3	$S_{wi} = 20\%$	0.3023
S4	$P_f = 0.1$ MPa	0.5448
S5	$P_f = 0.2$ MPa	0.6025
S6	$P_\pi = 0.33$ MPa	0.4266
S7	$P_\pi = 0.66$ MPa	0.4408

3.1 Effect of initial water saturation

The imbibition curves of shale samples at two different initial water saturation levels are shown in Fig. 7(a). From the figure, it can be seen that the higher the initial water saturation of the shale, the less the final imbibition volume. Theoretically, the imbibition rate depends on the net effect of capillary pressure and viscous resistance (Lucas, 1918). An increase in the initial water saturation may enhance the sample's mobility to water due to the increased wettability of water for the rock, but it also reduces the capillary pressure gradient (driving force). During the first two imbibition stages, capillary pressure controls the imbibition process, with dry samples having the highest capillary pressure gradient. As a result, the dry sample soaks up water faster than the other two samples during this period. During the period of imbibition

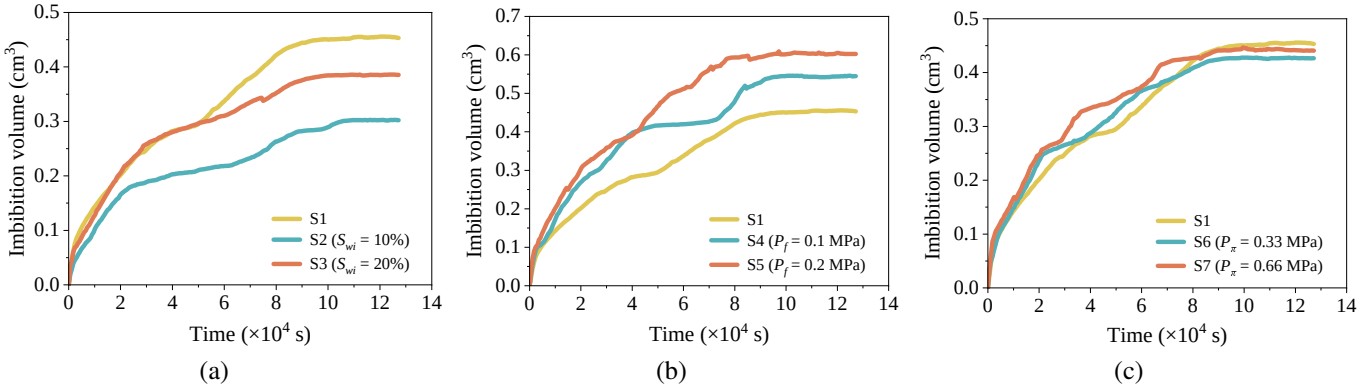

Fig. 7. Imbibition curves of six shale samples at different conditions: (a) Water saturation, (b) driving pressure, and (c) osmotic pressure.

balance, it can be observed that the imbibition rates of the three samples gradually decrease and eventually reach equilibrium.

3.2 Effect of driving pressure

It can be seen from Fig. 7(b) that variation in driving pressure affects the shale imbibition volume. The main difference between forced imbibition and normal pressure imbibition lies in the imbibition diffusion stage and imbibition transformation stage. With the increase in driving pressure, the slope of the imbibition curve in the imbibition diffusion stage gradually increases. When the dry sample undergoes imbibition under normal pressure for 25 hours, it reaches the critical time and imbibition volume without significant changes. In contrast, the S4 and S5 samples have a certain degree of increase in the imbibition volume at the late stage of imbibition, and at the end of the experiment, there is a significant increase in the final imbibition volume compared with that of the dry samples. Under driving pressures of 0, 0.1 and 0.2 MPa, the final imbibition volumes of shale samples were respectively 0.4073, 0.5448 and 0.6025 cm^3.

3.3 Effect of osmotic pressure

Typically, original formation water in shale reservoirs has high mineralization rate, and when it comes into contact with low-mineralization fracturing fluids, imbibition occurs due to chemical potential differences. Fig. 7(c) shows the imbibition volume variation of shale over time at different osmotic pressures. From the figure, it can be observed that the higher the osmotic pressure, the stronger the imbibition capability, resulting in a larger final imbibition volume. Therefore, the reduction in the salinity of fracturing fluid can appropriately increase the osmotic pressure difference and strengthen the imbibition effect in engineering applications.

3.4 Analysis of the influencing factors

The volume of imbibition was analyzed as the dependent variable, and various factors influencing the imbibition effect were analyzed as independent variables, using the multiple linear regression method and Statistical Package for the Social Sciences mathematical statistical analysis software. Regression analysis was conducted to obtain the correlation coefficient of each influencing factor. Based on the magnitude of the correlation coefficient, the degree of influence of each factor on the imbibition effect was determined.

Table 5. The correlation coefficient of different factors on the effect of imbibition.

No.	Influencing factor	Correlation coefficient
1	Osmotic pressure	0.589
2	Initial water saturation	0.093
3	Driving pressure	0.583

The multiple linear regression method is suitable for studying the relationship between one dependent variable and multiple independent variables, with the specific equation as follows:

$$Y = \beta_0 + \beta_1 X_1 + \beta_2 X_2 + \cdots + \beta_P X_P + \alpha \quad (1)$$

where Y is the dependent variable, $X_1, X_2, \cdots, X_P$ are the independent variable, α is a random error, $\beta_0, \beta_1, \ldots, \beta_P$ are the correlation coefficient.

The experimental data were imported into the linear regression statistical analysis module of Statistical Package for the Social Sciences mathematical statistical analysis software. The independent variables were set as osmotic pressure, driving pressure and initial water saturation, while the dependent variable was imbibition volume. Table 5 shows the correlation coefficients and the degree of influence of each factor on the imbibition volume. From the calculation results, it can be inferred that osmotic pressure is the main controlling factor affecting imbibition volume.

4. Discussion

4.1 Model derivation

4.1.1 Imbibition forces in underground engineering

In this section, the effects of osmotic pressure, driving pressure and initial water saturation on imbibition are qualitatively analyzed, and these three parameters are introduced into the

Table 6. Input parameters for the new imbibition model.

Parameter	Unit	Value
Sample cross-sectional area (A)	cm^2	4.92
Sample volume (V)	cm^3	24.83
Interfacial tension of water (σ)	mN/m	72.58
Viscosity of water (μ_w)	Pa·s	1.01
Porosity (ϕ)	%	3.41
Capillary pressure (P_f)	MPa	7.19
Average pore radius (r)	nm	19.13
Permeability (K)	D	2.3×10^{-6}

traditional Handy model to better describe the forced imbibition process under actual engineering conditions.

4.1.2 Osmotic pressure

Osmotic pressure is one of the main driving forces of shale imbibition (Fakcharoenphol et al., 2013; Wang and Pan, 2016; Chen and Wang, 2021; Uzun and Kazemi, 2021). Shale reservoirs are characterized by a high brine content of up to 280,000 pm; however, water-based fracking fluids have a low salinity of about 1,000 pm (Wang et al., 2018). Chemical osmosis can take place in the presence of a semipermeable membrane and differences in salinity. In geological research, these membranes are composed of clay minerals (McKelvey and Milne, 1960; Young and Low, 1965; Kemper and Rollins, 1966; Groenevelt and Elrick, 1976). The effect of osmotic pressure on shale imbibition must be taken into account during hydraulic fracturing under engineering conditions. In actual engineering application, a large volume of low-salinity water enters the reservoir that creates a salinity difference with the in-situ water present, which produces osmosis near the pores.

4.1.3 Driving pressure

Under engineering conditions, shale pores are affected not only by capillary force and osmotic pressure but also by driving pressure. In the process of hydraulic fracturing, the fluid in the fracture will be subjected to a certain pressure, which is jointly acted by of the overlying rock layer and the pumping pressure.

4.1.4 Initial water saturation

Initial water saturation is one of the critical parameters in reservoir engineering (Li and Li, 2014). The rate of spontaneous imbibition could be significantly affected by the initial water saturation, due to its impact on capillary pressure and viscous resistance to the reservoir fluid (Akin et al., 2000; Hu et al., 2002; Li et al., 2006; Cai et al., 2010). The higher the initial water saturation of the shale, the more void space it will occupy, resulting in less free gas.

4.1.5 Modified model

Integrating the above three influencing factors into the traditional Handy model can yield a new imbibition model, which considers the osmotic pressure, the driving pressure, and the initial water saturation as critical parameters.

The traditional Handy imbibition model is expressed as:

$$Q^2 = \frac{2A^2 P_c K \phi S_{wf}}{\mu_w} t \tag{2}$$

Taking the traditional Handy model as a basis, the above influencing factors are introduced to obtain a new imbibition model:

$$Q^2 = \frac{2A^2 (P_c + P_f + P_\pi) K \phi (S_{wf} - S_{wi})}{\mu_w} t \tag{3}$$

4.2 Comparison of model calculation and experimental result

In order to verify the accuracy of the new model, Table 6 lists the parameter values used as inputs to the model, and by adding these to the new model, comparison plots between the experimental data and the model simulation results are obtained (Fig. 8).

The results show that the simulated imbibition volume of the six experimental samples fits the experimental data well in the first two stages of imbibition, which accounts for 90% of the total imbibition volume. In the imbibition balance stage, the new model has a poor fit, which may be related to the boundary effect of the samples. The imbibition balance stage is characterized by restricted imbibition, which depends on the boundary conditions of the sample. However, this stage is possible in real reservoirs because the reservoir can be considered as having no boundary conditions compared to a finite amount of fracturing fluid. In other words, the simulation results of the imbibition balance stage can reflect the imbibition capacity under reservoir conditions. Therefore, the new imbibition model has better applicability under reservoir conditions.

4.3 Comparison with traditional models

In order to further analyze the validity of the model, the simulation results of the new model were compared with two existing imbibition models (the Benavente model and the traditional Handy model) (Fig. 9 roundness of δ = 1.21 and tortuosity of τ = 2.13 are adopted in the Benavente model. Other parameters required by these models are listed in Table 6.). The linear regression results indicate that the new model has the best fit throughout the imbibition process (R^2 = 0.9591). As shown in Fig. 9, the imbibition balance stage has a poor fit, while the imbibition diffusion stage and imbibition transformation stage represent the true imbibition capacity of the sample. Thus, it can be concluded that the new model has good applicability and accuracy in simulating the imbibition behavior of shale. The simulation results for different initial water saturations showed that those of the traditional Handy model were higher than the experimental data. This is because the initial water saturation will reduce the imbibition ability of the shale, which is not considered in the traditional Handy model. The comparison of simulations for osmotic pressure and driving pressure show that the results of the traditional Handy model are lower than the experimental data. This is because the increase in osmotic pressure and

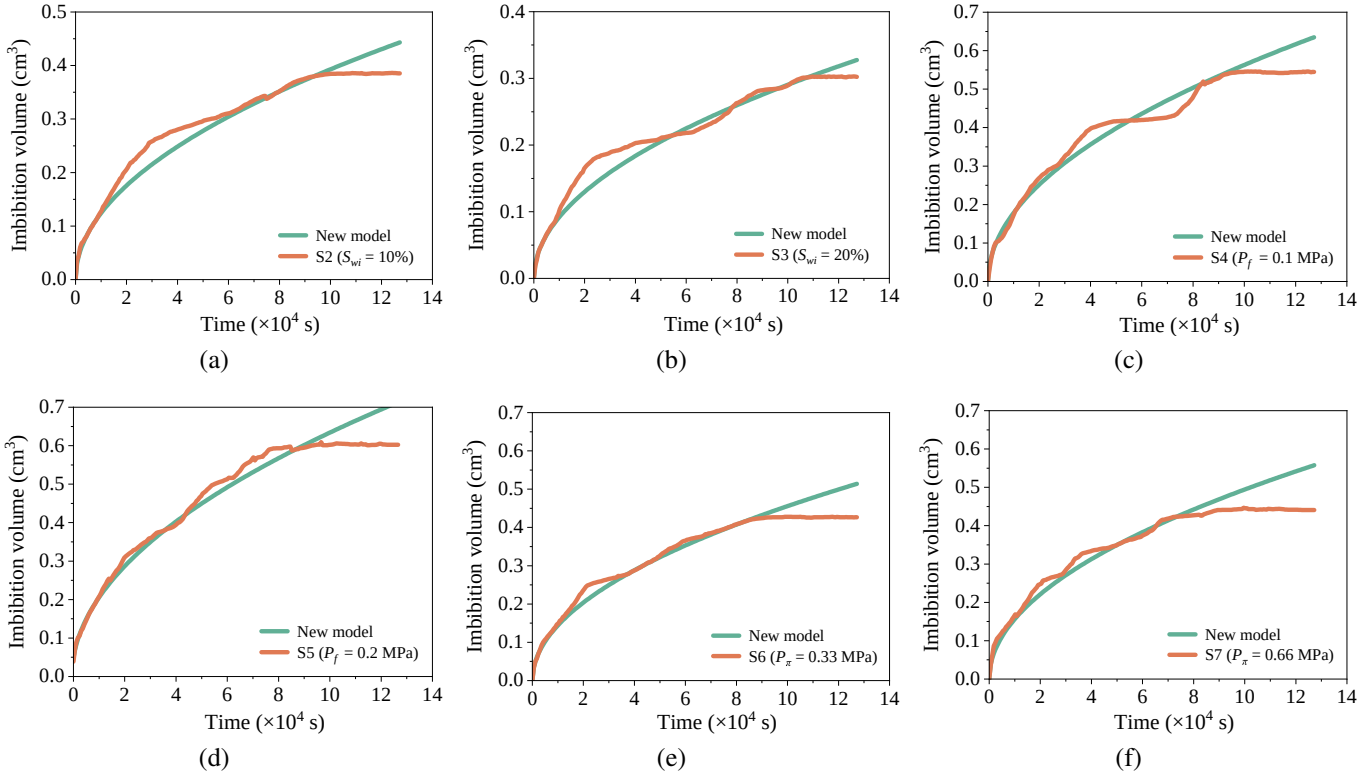

Fig. 8. Comparison of experimental data and model simulation results: (a) to (f) correspond to S2 to S7.

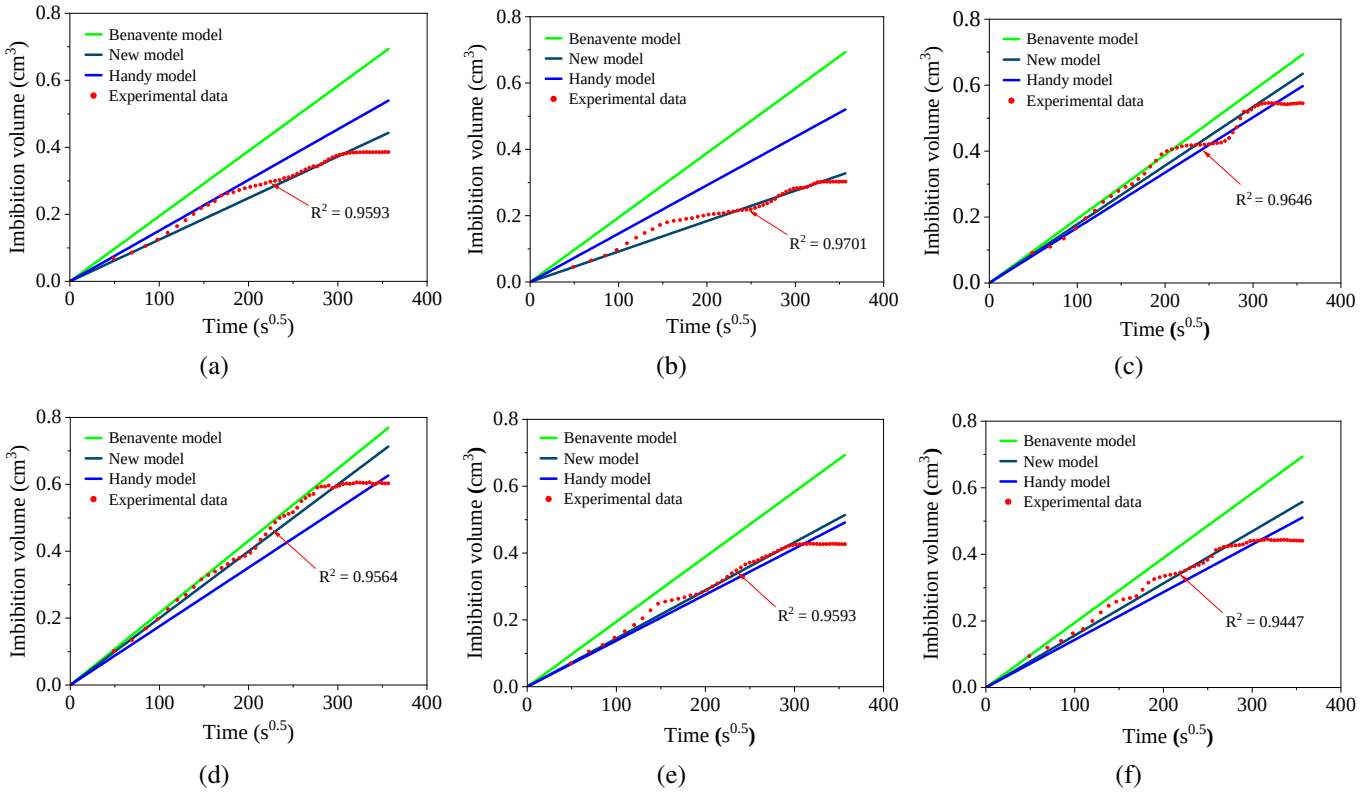

Fig. 9. Comparison of experimental data for samples S2-S7 and simulation results from three imbibition models: (a) to (f) correspond to S2 to S7.

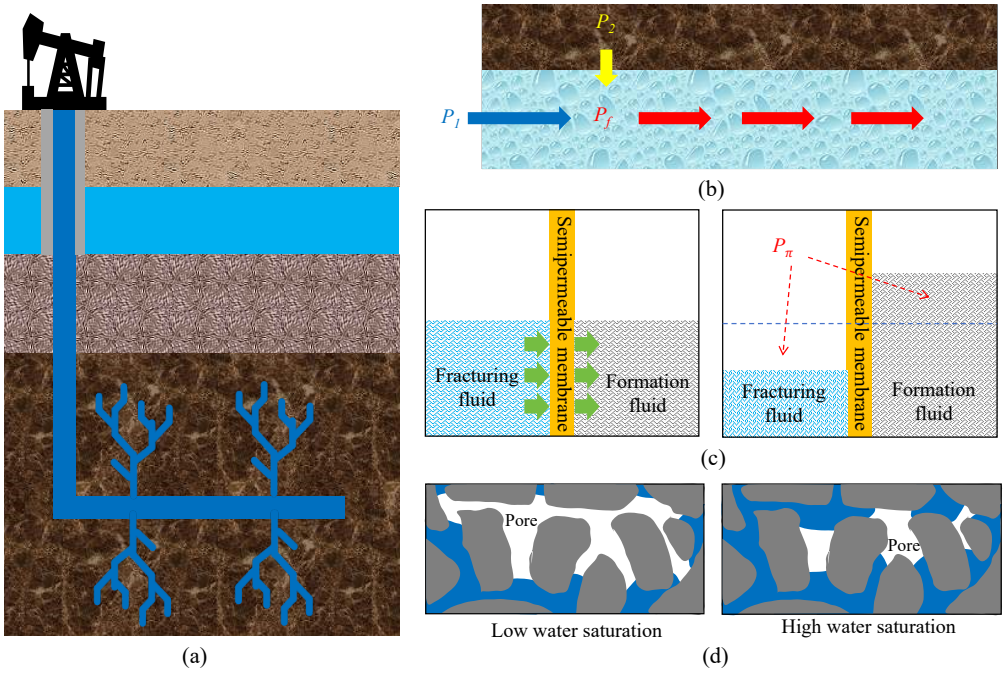

Fig. 10. Influencing factors of the imbibition effect: (a) Hydraulic fracturing engineering, (b) driving pressure, (c) osmotic pressure, and (d) initial water saturation.

driving pressure can increase the imbibition capacity of shale, indicating that the traditional Handy model underestimates the imbibition capacity of shale under actual reservoir conditions. The Benavente model predicts a higher imbibition volume than our new model. This is due to the experimental selection of complex shale core samples, which are formed with complex pore networks. In contrast, the classical empirical formulas for roundness and tortuosity can only represent the average pore state. Therefore, the Benavente model may have overestimated the imbibition capacity of samples in this experiment, resulting in a high predicted imbibition volume. Compared with the existing model, the new model can better simulate the imbibition process for dense shale reservoirs.

4.4 Engineering analysis

Hydraulic fracturing is an important technical measure to increase production in oil and gas wells and injection wells (Fig. 10(a)). It uses a surface high-pressure pump group to push fracturing fluid into the well, holding high pressure at the bottom of the well. When this pressure overcomes the stress near the wellbore and reaches the tensile strength of the rock, one or more fractures will be generated at the bottom of the well. During hydraulic fracturing, the fluid in the fracture often bears the combined pressure of pump pressure (P_1) and overlying rock layer pressure (P_2), which to some extent affects the imbibition effect (Fig. 10(b)).

Osmotic pressure is an additional important factor affecting the spontaneous imbibition effect. Shale reservoirs have high brine content of up to 280,000 pm, while the salinity of water-based fracturing fluid is approximately 1,000 pm. When there is a significant difference in brine content between fracturing fluid and reservoir formation water, water molecules from the low-salinity fluid enter the reservoir through a semi-permeable membrane constructed of clay minerals under osmotic pressure, driving the gas phase out of the pores and enhancing the imbibition effect (Fig. 10(c)). Initial water saturation is one of the key parameters in reservoir engineering. The higher the initial water saturation of shale, the larger the pore space it occupies and the lower the imbibition efficiency. Understanding the relationship between initial water saturation and imbibition effect is crucial for water injection engineering (Fig. 10(d)).

5. Conclusions

1) Based on the imbibition experimental data of seven shale core samples and the multiple linear regression analysis method, osmotic pressure had the greatest impact on shale imbibition, with a correlation coefficient of 0.589. The correlation coefficients between initial water saturation and driving pressure were 0.093 and 0.583, respectively.
2) A new mathematical model has been established to describe the dynamic imbibition behavior. The results of imbibition experiments on seven shale core samples show that the new model has high fitting accuracy. Furthermore, when compared with existing imbibition models, the new model has higher fitting accuracy.

Acknowledgements

The authors gratefully acknowledge the funds provided by Guizhou Provincial Science and Technology Projects (Nos. Qian Science Foundation-ZK [2022] 106, CXTD [2022] 016, and ZK [2023] 192).

Conflict of interest

The authors declare no competing interest.

References

Abd, A. S., Elhafyan, E., Siddiqui, A. R., et al. A review of the phenomenon of counter-current spontaneous imbibition: Analysis and data interpretation. Journal of Petroleum Science and Engineering, 2019, 180: 456-470.

A, Hu., Yang, Z., Hu, R., et al. Roles of energy dissipation and asymmetric wettability in spontaneous imbibition dynamics in a nanochannel. Journal of Colloid and Interface Science, 2022, 607: 1023-1035.

Akin, S., Schembre, J. M., Bhat, S. K., et al. Spontaneous imbibition characteristics of diatomite. Journal of Petroleum Science and Engineering, 2000, 25(3-4): 149-165.

Benavente, D., Lock, P., Ángeles García Del Cura, M., et al. Predicting the capillary imbibition of porous rocks from microstructure. Transport in Porous Media, 2002, 49: 59-76.

Cai, J., Perfect, E., Cheng, C., et al. Generalized modeling of spontaneous imbibition based on hagen-Poiseuille flow in tortuous capillaries with variably shaped apertures. Langmuir, 2014, 30(18): 5142-5151.

Cai, J., Yu, B., Zou, M., et al. Fractal characterization of spontaneous co-current imbibition in porous media. Energy & Fuels, 2010, 24(3): 1860-1867.

Chakraborty, N., Karpyn, Z. T., Liu, S., et al. Permeability evolution of shale during spontaneous imbibition. Journal of Natural Gas Science and Engineering, 2017, 38: 590-596.

Chen, Q., Wang, F. The flowback behavior of salt in hydraulically fractured shale under multi-phase flow conditions: Modelling, simulation and application. Journal of Natural Gas Science and Engineering, 2021, 4: 103985.

Deng, L., Pan, Y. Application of physics-informed neural networks for self-similar and transient solutions of spontaneous imbibition. Journal of Petroleum Science and Engineering, 2021, 203: 108644.

Fakcharoenphol, P., Torcuk, M. A., Wallace, J., et al. Managing shut-in time to enhance gas flow rate in hydraulic fractured shale reservoirs: A simulation study. Paper SPE 166098 Presented at SPE Annual Technical Conference and Exhibition, New Orleans, Louisiana, 30 September-2 October, 2013.

Gao, L., Yang, Z., Shi, Y. Experimental study on spontaneous imbibition characteristics of tight rocks. Advances in Geo-Energy Research, 2018, 2(3): 292-304.

Gao, Z., Fan, Y., Hu, Q., et al. A review of shale wettability characterization using spontaneous imbibition experiments. Marine and Petroleum Geology, 2019, 109: 330-338.

Ghanbari, E., Dehghanpour, H. Impact of rock fabric on water imbibition and salt diffusion in gas shales. International Journal of Coal Geology, 2015, 138: 55-67.

Groenevelt, P. H., Elrick, D. F. Coupling phenomena in saturated homo-ionic montmorillonite: I. Experimental. Soil Science Society of America Journal, 1976, 40: 820-823.

Gruener, S., Hermes, H. E., Schillinger, B., et al. Capillary rise dynamics of liquid hydrocarbons in mesoporous silica as explored by gravimetry, optical and neutron imaging: Nano-rheology and determination of pore size distributions from the shape of imbibition fronts. Colloids Surfaces A: Physicochemical and Engineering Aspects, 2016, 496: 13-27.

Handy, L. Determination of effective capillary pressures for porous media from imbibition data. Transactions of the AIME, 1960, 219(1): 75-80.

Hassan, A., Bruining, H., Musa, T., et al. The use of RFID technology to measure the compositions of diethyl ether oil-brine mixtures in enhanced imbibition experiments. Journal of Petroleum Science and Engineering, 2017, 156: 769-779.

Hu, Q., Kneafsey, T. J., Trautz, R. C., et al. Tracer penetration into welded tuff matrix from flowing fractures. Vadose Zone Journal, 2002, 1(1): 102-112.

Hu, Y., Zhao, C., Zhao, J., et al. Mechanisms of fracturing fluid spontaneous imbibition behavior in shale reservoir: A review. Journal of Natural Gas Science and Engineering, 2020, 82: 103498.

Kemper, W. D., Rollins, J. B. Osmotic efficiency coefficients across compacted clays. Soil Science Society of America Journal, 1966, 30(5): 529-534.

Lai, F., Li, Z., Wei, Q., et al. Experimental investigation of spontaneous imbibition in a tight reservoir with nuclear magnetic resonance testing. Energy & Fuels, 2016, 30: 8932-8940.

Li, G., Su, Y., Wang, W., et al. Mathematical model and application of spontaneous and forced imbibition in shale porous media-considered forced pressure and osmosis. Energy & Fuels, 2022, 36: 5723-5736.

Li, K., Chow, K., Horne, R. N. Influence of initial water saturation on recovery by spontaneous imbibition in gas/water/rock systems and the calculation of relative permeability. SPE Reservoir Evaluation & Engineering, 2006, 9(4): 295-301.

Li, K., Li, Y. Effect of initial water saturation on crude oil recovery and water cut in water-wet reservoirs. International Journal of Energy Research, 2014, 38(12): 1599-1607.

Li, Y., Hu, Z., Cai, C., et al. Evaluation method of water saturation in shale: A comprehensive review. Marine and Petroleum Geology, 2021, 128: 105017.

Lucas, R. Ueber das aeitgesetz des kapillaren aufstiegs von flussigkeiten. Kolloid-Zeitschrift, 1918, 23: 15-22.

McKelvey, J. G., Milne, I. H. The flow of salt solution through compacted clay. Clays and Clay Minerals, 1960, 9: 248-259.

Neunkirchen, S., Blößl, Y., Schledjewski, R. A porous capillary tube approach for textile saturation. Composites Science and Technology, 2022, 2: 109450.

Schmid, K. S., Geiger, S. Universal scaling of spontaneous imbibition for water-wet systems. Water Resources Research, 2012, 48(3): W03507.

Uzun, O., Kazemi, H. Assessment of enhanced oil recovery by osmotic pressure in unconventional reservoirs: Application to Niobrara chalk and Codell sandstone. Fuel, 2021, 306: 121270.

Wang, F., Pan, Z., Zhang, Y., et al. Simulation of coupled hydro-mechanical-chemical phenomena in hydraulically fractured gas shale during fracturing-fluid flowback. Journal of Petroleum Science and Engineering, 2018, 163: 16-26.

Wang, F., Pan, Z. Numerical simulation of chemical potential dominated fracturing fluid flowback in hydraulically fractured shale gas reservoirs. Petroleum Exploration and Development, 2016, 43 (6): 1060-1066.

Wang, H., Yang, L., Wang, S., et al. Study on imbibition characteristics of glutenite with different boundary conditions based on NMR experiments. Energy & Fuels, 2022a, 36: 14101-14112.

Wang, K., Li, Z., Ye, K., et al. A new dynamic imbibition model for penny-shaped blind pores in shale gas well. Journal of Natural Gas Science and Engineering, 2022b, 101: 104553.

Wang, X., Wu, N., Su, Z., et al. Progress of the enhanced geothermal systems (EGS) development technology. Progress in Geophysics, 2012, 27(1): 0355-62.

Washburn, E. W. The dynamics of capillary flow. Physical Review, 1921, 17: 273-283.

Xu, G., Shi, Y., Jiang, Y., et al. Characteristics and influencing factors for forced imbibition in tight sandstone based on low-field nuclear magnetic resonance measurements. Energy & Fuels, 2018, 32(8): 8230-8240.

Young, A., Low, P. F. Osmosis in argillaceous rocks. AAPG Bulletin, 1965, 49(7): 1004-1008.

Yuan, X., Yao, Y., Liu, D., et al. Spontaneous imbibition in coal: Experimental and model analysis. Journal of Natural Gas Science and Engineering, 2019, 67: 108-121.

Zeng, F., Zhang, Q., Guo, J., et al. Analytical spontaneous imbibition model for confined nanofractures. Journal of Geophysics and Engineering, 2020, 17: 635-642.

Zhao, Z., Jiang, Z., Guo, J., et al. A new multi-pore fractal model to delineate the effect of various factors on imbibition in shales. Fuel Communications, 2021, 7: 100012.

Zhou, Z., Abass, H., Li, X., et al. Mechanisms of imbibition during hydraulic fracturing in shale formations. Journal of Petroleum Science and Engineering, 2016, 141: 125-132.